IEEE Access
Multidisciplinary | Rapid Review | Open Access Journal

Received September 22, 2020, accepted October 12, 2020, date of publication October 15, 2020, date of current version October 27, 2020.

Digital Object Identifier 10.1109/ACCESS.2020.3031471

Noninvasive Monitoring of Potassium Fluctuations During the Long Interdialytic Interval

ANA SANTOS RODRIGUES[1], ANDRIUS PETRĖNAS[1], BIRUTĖ PALIAKAITĖ[1], NEDA KUŠLEIKAITĖ-PERE[2,3], GEDIMINAS JARUŠEVIČIUS[4], INGA ARŪNĖ BUMBLYTĖ[2,3], PABLO LAGUNA[5,6], (Fellow, IEEE), AND VAIDOTAS MAROZAS[1,7], (Member, IEEE)

[1]Biomedical Engineering Institute, Kaunas University of Technology, 51423 Kaunas, Lithuania
[2]Department of Nephrology, Faculty of Medicine, Medical Academy, Lithuanian University of Health Sciences, 50009 Kaunas, Lithuania
[3]Department of Nephrology, Hospital of Lithuanian University of Health Sciences Kaunas Clinics, 50161 Kaunas, Lithuania
[4]Institute of Cardiology, Medical Academy, Lithuanian University of Health Sciences, 50161 Kaunas, Lithuania
[5]Biomedical Signal Interpretation and Computational Simulation (BSICoS) Group, Aragón Institute of Engineering Research (I3A), IIS Aragón, University of Zaragoza, 50018 Zaragoza, Spain
[6]Biomedical Research Networking Center (CIBER), 50018 Zaragoza, Spain
[7]Faculty of Electrical and Electronics Engineering, Kaunas University of Technology, 51367 Kaunas, Lithuania

Corresponding author: Ana Santos Rodrigues (ana.rodrigues@ktu.lt)

This work was supported by the European Regional Development Fund with the Research Council of Lithuania (LMTLT) under Project 01.2.2-LMT-K-718-01-0030.

ABSTRACT Hemodialysis patients are susceptible to life-threatening arrhythmias whose incidence is markedly higher during the long interdialytic interval due to electrolyte fluctuations. Noninvasive monitoring of electrolyte fluctuations, particularly those of potassium, would enable restoring electrolyte balance before the onset of arrhythmias. This study investigates the feasibility of continuous long-term monitoring of potassium fluctuations using a single-lead electrocardiogram. We evaluate patient-specific T-wave morphology changes in the electrocardiogram using two descriptors: 1) a model-based descriptor, θ_δ, developed to account for overall morphology changes, and 2) the currently available descriptor, T_{SA}, sensitive to potassium levels in single-lead electrocardiograms. Electrocardiograms of 15 hemodialysis patients with pre-existent cardiac diseases were acquired continuously over the long interdialytic interval along with blood samples at predetermined time instants. Results reveal that θ_δ and T_{SA} respond concordantly with potassium levels, and reacts to potassium lowering medication. The overlapping index of the daily distributions of θ_δ and T_{SA} are moderately correlated with changes in potassium levels ($r = -0.56$ and $r = -0.57$, respectively). θ_δ exhibits circadian variation, peaking amidst morning and decreasing until evening. θ_δ appears to be less affected by motion-induced noise, which is preferable for ambulatory monitoring. Although long-term monitoring of potassium fluctuations is feasible even in complicated hemodialysis patients, the presence of concomitant electrolyte (calcium and bicarbonate) imbalances should be accounted for since it can hamper a reliable estimation. Considering that intradialytic T-wave morphologies may differ from the ones manifested between hemodialysis sessions, future studies should also strive to collect blood samples outside of hemodialysis to improve electrolyte estimation methods.

INDEX TERMS Chronic kidney disease, electrolyte imbalance, hemodialysis, hyperkalemia, hypocalcemia, metabolic acidosis, sudden cardiac death, T-wave parametrization.

I. INTRODUCTION

Hemodialysis (HD) patients have a considerably higher risk of sudden death due to cardiac arrhythmias, such as extreme bradycardia and ventricular tachycardia [1], which are more frequent during the long interdialytic interval [2]–[4]. Electrolyte fluctuations, particularly those of potassium, are reckoned to be among the primary triggers of these dangerous arrhythmias [2], [4]. Unfortunately, the asymptomatic nature of electrolyte fluctuations, along with the fact that blood

The associate editor coordinating the review of this manuscript and approving it for publication was Mohammad Zia Ur Rahman.

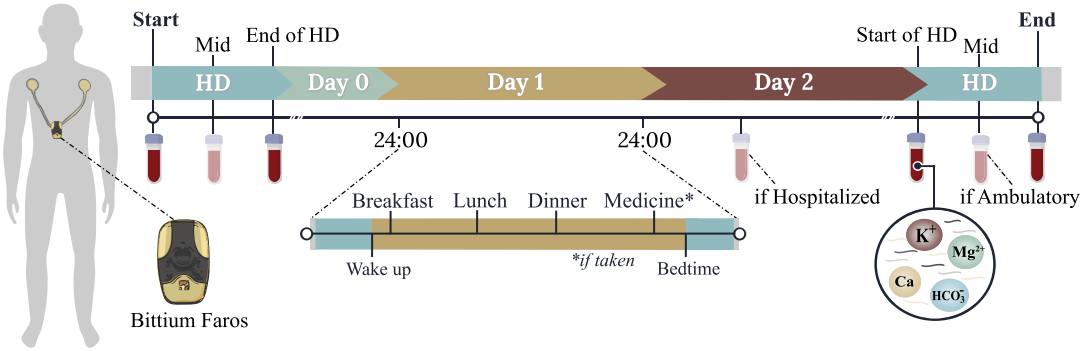

FIGURE 1. Data acquisition protocol. Lead-I ECG signals of hospitalized and ambulatory patients were acquired throughout the long interdialytic interval using an ambulatory recorder. Blood samples of hospitalized patients were collected twice during each HD (start and end) and at least once during the long interdialytic interval. Blood samples of ambulatory patients were collected only through the course of each HD (start, mid, and end).

testing is neither routinely requested, nor can be performed at home, often engenders life-threatening conditions [4]. Accordingly, long-term noninvasive monitoring of electrolyte fluctuations could be of clinical importance [5], [6] as it would allow a timely correction of electrolyte imbalance by performing early HD.

Electrolyte fluctuations are often reflected in the electrocardiogram (ECG) since non-homeostatic serum electrolyte levels perturb the resting membrane potential of heart cells [7], [8]. For instance, an altered T-wave morphology, caused by disturbances in ventricular repolarization, is a manifestation of anomalous serum potassium [8], [9]. However, identifying electrolyte fluctuations from an ECG is challenging [10], [11], especially if no baseline ECG is available for comparison [12], mainly due to confounding factors, such as cardiovascular comorbidities, medications or concurrent electrolyte imbalances, that mask or mimic the anticipated ECG alterations [9], [12]. The ambiguity of the emblematic ECG features profoundly contributes to the low ECG specificity, particularly when cardiovascular comorbidities are present [10]. Thus, exploring ECG-derived descriptors with higher specificity to serum electrolyte levels is crucial for noninvasive monitoring of electrolyte fluctuations.

A pioneering 12-lead ECG-based descriptor, T_{SA}, was proposed for the quantification of serum potassium during HD [13]. Mayo Clinic researchers further enhanced the descriptor for use in a single-lead ECG, first precordial [14], [15], and later in lead-I acquired from a handheld device [16]. The descriptor was further compared to another descriptor, which evaluates the complete T-wave morphology [17], and studied under electrophysiological modeling [18]. Albeit with encouraging results, these studies investigated the descriptors' performance exclusively during HD procedures; thus, the feasibility of long-term ambulatory monitoring of potassium fluctuations remains unexplored. In interdialytic settings, serum electrolyte levels may fluctuate more gradually than during HD, where electrolyte levels usually are corrected in approximately 4 h. Rapid fluctuations of serum electrolyte levels induce cardiac instability [19], resulting in noticeable T-wave morphology changes [20], [21], as typically seen throughout HD. However, when electrolyte levels vary slowly, such changes are less apparent and may not be distinctively quantifiable, especially in HD patients who may develop compensatory mechanisms or manifest antagonist electrolyte levels that stabilize the cardiac membrane potential [19].

This study explores the feasibility of capturing potassium fluctuations over the long interdialytic interval using a single-lead ECG. The study aims to understand the current challenges of long-term noninvasive monitoring of such fluctuations during activities of daily living where: (i) potassium may fluctuate slowly, (ii) concomitant electrolyte imbalance may arise, and (iii) underlying cardiac diseases prevail. Considering that potassium fluctuations may affect the overall T-wave morphology and T_{SA} relies on local T-wave features, we developed a model-based descriptor to account for global T-wave morphology. In contrast to other studies, we tracked T-wave morphology changes continuously between HD sessions in patients with several cardiac diseases as a realistic representation of the HD population. We investigate in detail patient-specific responses of T-wave morphology changes to gradual electrolyte fluctuations. In adition, we tested the performance of the descriptors in different signal quality periods.

This paper is organized as follows. Firstly, we describe a model-based descriptor to monitor serum potassium fluctuations in a single-lead ECG. Secondly, we present results on a database recorded during the long interdialytic interval. The paper ends with considerations for future research, followed by conclusions.

II. METHODS

A. DATA COLLECTION

Seventeen HD patients (9 females, age 57.4 $\pm$ 14.6 years), hospitalized or ambulatory, from the Hospital of Lithuanian University of Health Sciences Kaunas Clinics, were eligible for this study. The study was approved and carried out following the recommendations of the Kaunas Regional Biomedical Research Ethics Committee (#BE-2-43), including written

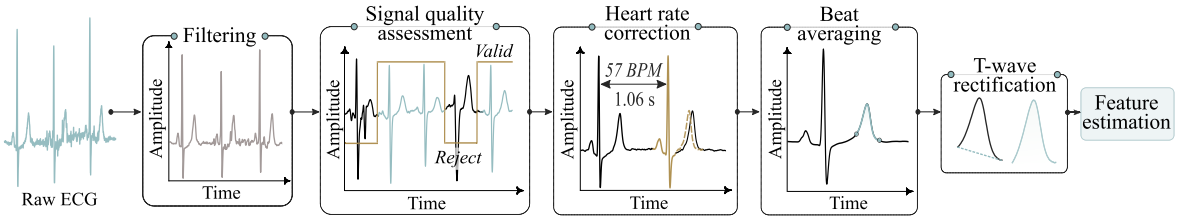

FIGURE 2. Preprocessing of a single-lead ECG.

informed consent from all patients per the Declaration of Helsinki.

Hospitalized patients were not bedridden and were free to move in hospital facilities. Lead-I ECG was acquired during the long interdialytic interval (∼71 h for each patient, a total of ∼1078 h) using Bittium Faros (Bittium Corporation, Oulu, Finland) ambulatory recorder at a sampling rate of 500 Hz. Data acquisition started before the last HD of the week, either Friday or Saturday, and ended after the following HD on Monday or Tuesday (Fig. 1). From this point onwards, Friday HD refers to the last HD of the week, whereas Monday HD denotes the following HD.

Blood samples were drawn twice (start and end) during each HD procedure from hospitalized patients, and thrice (start, mid, and end) from ambulatory patients to assess serum potassium ($[K^+]$), magnesium ($[Mg^{2+}]$), calcium ([Ca]) and bicarbonate ($[HCO_3^-]$) levels. At least one additional blood sample between HD sessions was collected from hospitalized patients at a predetermined time instant, decided by the physician on call. All patients were also asked to register the time of meal and medication intake.

Out of 17 patients, two were excluded from the analysis. One patient presented ventricular tachycardia episodes during the recording and was taken to the intensive care unit, while the other terminated recording just a few hours after Friday HD due to discomfort. Two hospitalized patients required urgent HD one day earlier. Patients were divided into two groups: *Group I* comprises patients with regular sinus rhythm and high signal quality over the whole recording period, whereas *Group II* includes patients whose recordings were noisy, with arrhythmias or affected by ingestion of potassium-lowering medication (Sorbisterit). Patients in both groups manifested concomitant electrolyte imbalances (calcium, bicarbonate, and magnesium). Table 1 provides patient and recording characteristics.

B. ECG PREPROCESSING

The recorded ECGs underwent preprocessing comprised of filtering, signal quality assessment, heart rate-based correction of T-wave duration, beat averaging, and T-wave rectification (Fig. 2).

1) FILTERING

For a reliable assessment of electrolyte fluctuations, it is crucial to avoid distortions in the ST-segment and T-wave. Thus, the ECGs were filtered using a combination of high-order finite impulse response filters. Baseline wandering was removed by using an 836^{th} order high-pass filter with a cut-off frequency of $f_c = 0.6$ Hz, whereas high-frequency noise was suppressed using a 16^{th} order low-pass filter with $f_c = 40$ Hz.

2) SIGNAL QUALITY ASSESSMENT

A 90-s sliding window with 10-s overlap was used to segment the ECGs, discarding heartbeats that did not fulfill the signal quality index (SQI) criteria proposed in [22]. Segments with more than 50% poor-quality beats were considered non-analyzable.

Each ECG was divided into three days: *Day 0*, covering the remaining hours of the same day after Friday HD (until 22:00), *Day 1*, and *Day 2* as the ensuing and last days of the long interdialytic interval, respectively. Since lying positions can considerably alter the ECG morphology [23], *Day 1* and *Day 2* range from 07:00 till 22:00 as patients were usually awake within this period and the likelihood of encountering a lying position was reasonably low. ECG segments within episodes of arrhythmogenic events were excluded from the analysis.

3) HEART RATE CORRECTION

T-wave morphology is sensitive to heart rate changes, which must be rectified before evaluating the influence of serum electrolyte levels. Thus, the ST-T complex duration was resampled to fit the current RR interval, according to Fridercia's formula [24].

4) BEAT AVERAGING

The resampled heartbeats were aligned and averaged within each 90-s segment, resulting in a single representative heartbeat. QRS complex and T-wave onset were delineated using *ecg-kit* toolbox [25], whereas T-wave offset as described in [26]. Feature estimation was applied to the delineated T-waves of each averaged heartbeat.

5) T-WAVE RECTIFICATION

Each delineated T-wave, $T(n)$, was preprocessed through a series of steps to transform different waveforms as closely as possible to a positive T-wave. Accordingly, negative T-waves were inverted, $T(n) = -T(n)$. In waveforms with ST depression, the T-wave onset was amended to the local minimum

TABLE 1. Patient and recording characteristics.

	Patient characteristics			Recording characteristics		
	# / Type[1]	*Sex*[2]*/ Age*	*Comorbidities*[3]	*Electrolyte imbalance*[3]	*Total duration / High quality*	*Other notes*[4]
Group I	#1/A	F/69	Hypertension History of AF Diabetes	Hyperkalemia Hypermagnesemia	73.2 h / 92.6%	Frequent PVCs
	#2/A	F/68	Hypertension Ischemic heart disease: stable angina pectoris	Hyperkalemia Hypocalcemia (severe)	73.4 h / 93.2%	Frequent PVCs
	#3/H	F/52	Hypertension LVH Hyperparathyroidism	Hyperkalemia Hypocalcemia (mild)	75.6 h / 95.3%	
	#4/A	M/32	History of AF LVH	Metabolic acidosis Hypermagnesemia	73.7 h / 56.8%	
	#5/H	F/70	Hypertension Severe anemia	Hypocalcemia (severe) Metabolic acidosis	55.8 h / 77.2%	IV iron infusions Blood transfusion Urgent start of HD
	#6/A	M/50	Hypertension LVH Ischemic heart disease Diabetes	Hypocalcemia (mild) Hypermagnesemia	74.7 h / 92.0%	
	#7/H	F/65	Hypertension Ischemic heart disease: stable angina pectoris LVH Severe anemia	Hypocalcemia (mild)	73.8 h / 73.1%	Blood transfusion before Friday HD
Group II	#8/H	F/69	Hypertension	Hyperkalemia Hypocalcemia (mild)	73.4 h / 65.1%	Paroxysmal AF
	#9/H	F/78	Ischemic heart disease	Hyperkalemia Hypocalcemia (mild)	69.8 h / 79.7%	PACs; Tachycardia Use of sorbisterit
	#10/H	M/29	Hypertension LVH	Hyperkalemia Hypocalcemia (mild) Metabolic acidosis	77.6 h / 44.9%	Tachycardia Use of sorbisterit
	#11/H	M/51	Hypertension	Hyperkalemia Hypocalcemia (severe) Metabolic acidosis	75.2 h / 97.2%	Use of sorbisterit
	#12/H	M/64	Hypertension Diabetes	Hypocalcemia (severe) Hypomagnesemia	75.9 h / 79.8%	
	#13/H	M/47	Hypertension Stroke	Hyperkalemia Hypocalcemia (mild) Metabolic acidosis	75.8 h / 94.9%	Concomitant electrolyte imbalance during the whole recording
	#14/H	F/54	None	Hypocalcemia (mild) Hypomagnesemia	54.7 h / 41.0%	Thrombosis during Friday HD Taken to minor surgery Tachycardia Urgent start of HD
	#15/A	M/79	Hypertension Chronic heart failure Ischemic heart disease LVH Diabetes	Metabolic alkalosis Hypermagnesemia	75.6 h / 96.2%	

[1] A: ambulatory; H: hospitalized.
[2] F: female; M: male.
[3] AF: atrial fibrillation; LVH: left ventricular hypertrophy; PVCs: premature ventricular contractions; PACs: premature atrial contractions; IV: intravenous; Sorbisterit (calcium polystyrene sulphonate) is a potassium-lowering medication.
[4] Imbalances displayed on the start of Monday HD. Hyperkalemia: $[K^+] \geqslant 5.5$ mmol/L; Hypocalcemia (severe): $[Ca] \leqslant 1.9$ mmol/L; Hypocalcemia (mild): $1.9 < [Ca] < 2.23$ mmol/L; Hypermagnesemia: $[Mg^{2+}] \geqslant 1.03$ mmol/L; Hypomagnesemia: $[Mg^{2+}] \leqslant 0.74$ mmol/L; Metabolic acidosis: $[HCO_3^-] < 22$ mmol/L; Metabolic alkalosis: $[HCO_3^-] \geq 26$ mmol/L.

amplitude point. Once the onset and offset were delineated, the T-wave baseline was corrected to begin and end at zero amplitude. A baseline was estimated by linear interpolation between T-wave onset and offset, and subtracted from $T(n)$. Then, $T(n)$ was standardized to counteract amplitude discrepancies caused by body position changes or pre-existent cardiac diseases:

$$T^z(n) = \frac{T(n) - \bar{x}}{s}, \quad \forall n, \tag{1}$$

where $T^z(n)$ denotes the standardized T-wave, $\bar{x}$ and s are the mean and standard deviation of $T(n)$, respectively. From this point onwards, $T^z(n)$ denotes the standardized T-wave, whereas $T(n)$ the baseline-removed T-wave.

C. T-WAVE PARAMETRIZATION

Model-based parametrization was employed to quantify electrolyte-induced changes in T-wave morphology. The T-wave, composed of two asymmetrical slopes—upward and downward—was modeled using a composite model of two functions to characterize each slope separately. The model, inspired by the one proposed in [27] and [28], and briefly described in [29], consisted of one Gaussian and one

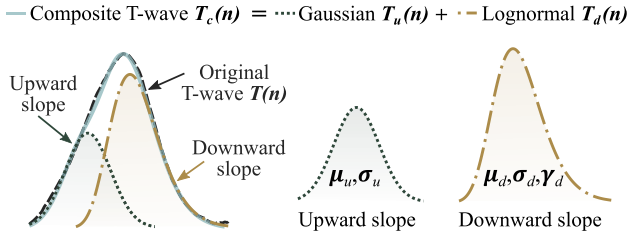

FIGURE 3. T-wave composite model.

lognormal functions (Fig. 3). The Gaussian function construed the upward slope and is defined by:

$$T_u(n; \sigma_u, \mu_u) = \frac{1}{\sqrt{2\pi\sigma_u^2}} e^{-\frac{(n-\mu_u)^2}{2\sigma_u^2}}, \tag{2}$$

where n represents sample number, μ_u and σ_u are the location and scale parameters. The lognormal function, which depicted the downward slope, is defined by:

$$T_d(n; \sigma_d, \mu_d, \gamma_d) = \frac{1}{(n-\gamma_d)\sigma_d\sqrt{2\pi}} e^{-\frac{(\ln(n-\gamma_d)-\mu_d)^2}{2\sigma_d^2}}, \tag{3}$$

where γ_d, μ_d and σ_d stands for the location, scale, and shape parameters, respectively. The time-shifting parameter γ_d ensures that $T_d(n)$ always fits the downward slope without modifying the shape and scale of the model. In this manner, we ensured an unambiguous reaction of μ_d and σ_d to morphological, but not temporal changes. $T(n)$ can then be characterized by combining (2) and (3) as:

$$T_c(n) = w_u T_u(n) + w_d T_d(n) + h. \tag{4}$$

The subscript c denotes the fitted composite model, whereas u and d imply that the parameters represent the upward and downward slopes. Both functions are weighted by parameters w_u and w_d, and balanced with an offset h. The parameters are merged into the vector $\boldsymbol{\phi} = [\sigma_u, \sigma_d, \mu_u, \mu_d, \gamma_d, w_u, w_d, h]$, which was estimated using the trust-region reflective least-squares algorithm with a set of empirically determined lower and upper boundaries to control the fitting process. Supplementary table 2 briefly presents such boundaries, along with values used to initialize $\boldsymbol{\phi}$. Before parameterization, $T(n)$ was resampled to 1000 samples, normalized to unit amplitude, and mirrored in time, $\widehat{T}(n) = T(-n)$. This step ensures that $\widehat{T}(n)$ becomes right-skewed as a lognormal, increasing the coefficient of determination R^2 and improving goodness of fit. Fitting is considered acceptable when R^2 exceeds the empirically chosen fixed threshold of 0.8. Otherwise, waves were considered of poor quality and thereby discarded from the analysis. Flat T-waves were excluded from the analysis since parametrization of such waves is unavailing. Figure 4 depicts T-wave rectification and parametrization for several ECG morphologies encountered in the data. Appendix B presents pseudocodes for the T-wave rectification and parametrization algorithms.[1]

[1]Note to readers: The code is available on GitHub. Repository name: T-waveModelPotassiumFluctuations

D. T-WAVE FEATURE ESTIMATION

When serum $[K^+]$ starts to rise above normal levels, the T-wave tends to become more peaked and decreases in duration [7], [9]. To quantify variations in T-wave peakedness, we estimated the angle θ between the upward and downward slopes (Fig. 5a-b). Assuming that each slope is defined as a line with gradient $\mathcal{S}$, θ was calculated by:

$$\theta = \beta - \alpha \equiv \arctan(\mathcal{S}_d) - \arctan(\mathcal{S}_u), \tag{5}$$

where β and α are the angles between the temporal axis and the downward and upward slope, whereas $\mathcal{S}_u$ and $\mathcal{S}_d$ are the gradients of the correspondent slopes. $\mathcal{S}_u$ and $\mathcal{S}_d$ were estimated from $T^z(n)$ in a similar way as in [30]: two lines were computed in an 8 ms window centered at the maximum gradient between T-onset and T-peak, and at the minimum gradient between T-peak and T-offset (Fig. 5c). $\mathcal{S}_u$ and $\mathcal{S}_d$ are the yielded gradients of the fitted lines in a.u./s.

As the duration of repolarization shortens, the T-wave becomes less elongated. Given that each function from the composite model depicts a slope, changes in T-wave elongation were characterized by a temporal displacement, δ, between the points of global maximum of $T_d(n)$ and $T_u(n)$ functions (Fig. 5d-e). Considering that the point of global maximum of a probability distribution is its mode, δ was found by:

$$\widehat{\delta} = m_d - m_u, \tag{6}$$

where m_d and m_u are the modes of lognormal and Gaussian functions. The mode of a Gaussian function is given by μ_u, whereas, for the three-parameter lognormal function, it was calculated as follows:

$$m_d = \gamma_d + e^{(\mu_d - \sigma_d^2)}. \tag{7}$$

Given that $\widehat{\delta}$ was estimated from the resampled $\widehat{T}(n)$, δ was amended to the original time scale:

$$\delta = \widehat{\delta}\frac{N}{1000}, \tag{8}$$

where N is the number of samples in $T(n)$. Conceptually, as serum $[K^+]$ starts to rise slowly during the long interdialytic interval, the T-wave becomes narrower and more peaked, translating into lower values of δ (s) and θ (°). Since θ and δ vary concordantly with each other, both decreasing when $[K^+]$ increases, we propose a new descriptor, θ_δ, that amplifies their response to serum $[K^+]$ fluctuations:

$$\theta_\delta = -\log_{10}(\theta \cdot \delta). \tag{9}$$

The logarithm expands the dynamic range and ensures that θ_δ is positively correlated with $[K^+]$ levels.

E. PERFORMANCE EVALUATION

The performance of the proposed descriptor, θ_δ, was compared to the descriptor introduced in [14]–[16], which was estimated as:

$$T_{SA} = \frac{\mathcal{S}_d}{\sqrt{T_A}}. \tag{10}$$

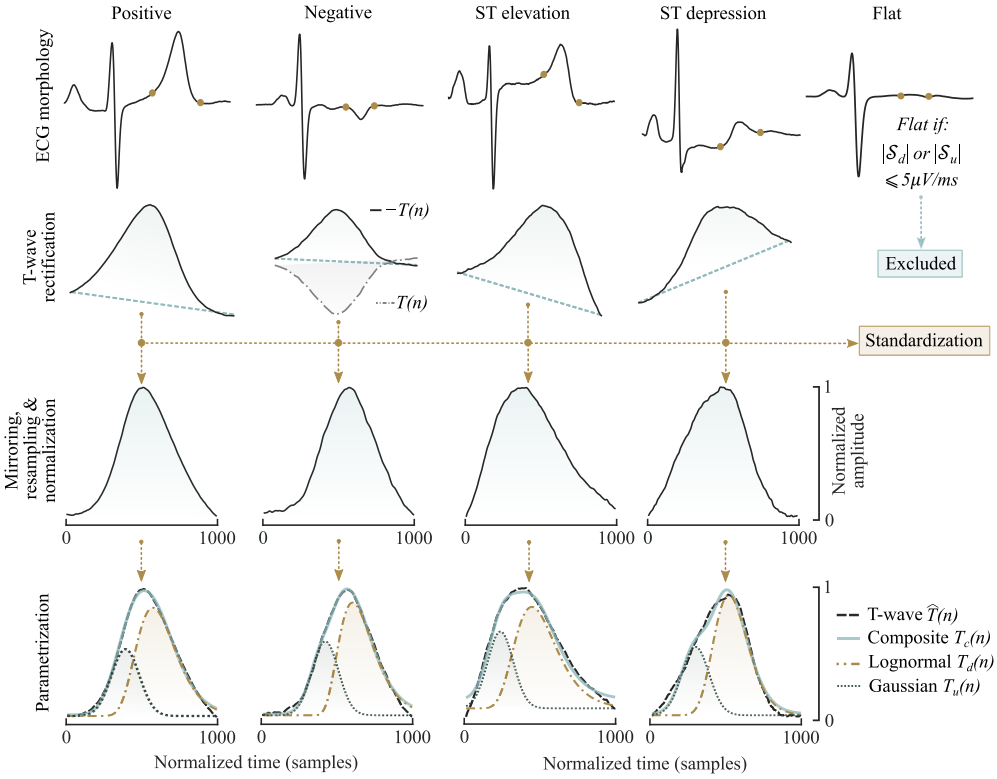

FIGURE 4. T-wave rectification and parametrization for various ECG morphologies encountered in the data. After delineating the T-waves for every valid averaged heartbeat, the T-wave was rectified, mirrored, resampled, normalized, and subjected to parametrization.

$\mathcal{S}_d$ (in a.u./s) is the downward slope and T_A is the peak-to-peak amplitude between the T-wave peak and offset. $\mathcal{S}_d$ and T_A were computed from the non-mirrored $T(n)$, normalized by the signal energy of its correspondent QRS-wave, as described in [15]. It should be noted that T_{SA} is not applicable for negative T-waves [15]. Despite being often used by clinicians to identify potassium abnormalities, the emblematic T-wave amplitude was not included for comparison, since it shows inferior performance to that of T_{SA} [14].

To examine the daily variation of θ_δ and T_{SA} relative to the $[K^+]$ reference values of each individual, kernel density estimations were used to obtain distributions of $\theta_\delta - \theta_{\delta_{t0}}$ and $T_{SA} - T_{SA_{t0}}$. The reference values were calculated at t_0 by finding the mean during the first 30 min following Friday HD termination. Within this 30 min period, $[K^+]$ remains nearly unchanged as none of the patients had a meal, thus avoiding insulin spikes that drive serum $[K^+]$ intracellularly [31].

The overlapping index η [32] was used to quantify similarities between the daily distributions of θ_δ and T_{SA}. The index η can take values between zero and one, where $\eta = 1$ indicates that the two distributions are identical. Intuitively, it is expected that higher $[K^+]$ fluctuations will translate into smaller η values. The relationship between η and $\Delta[K^+]$ was assessed using Pearson's correlation coefficient (r), where $\Delta[K^+]$ is expected to be negatively correlated with η. η was calculated between the days with assessed $[K^+]$, which, for the majority of patients, is solely between *Day 0* and *Day 2*. Since blood was collected at the start of Monday HD, *Day 2* distribution includes 2 h preceding Monday HD as well. The subscript of η specifies the days between which η is evaluated, whereas $\Delta[K^+]$ denotes the difference of $[K^+]$ between two days.

To investigate noise robustness of θ_δ and T_{SA} in more detail, we compared the coefficient of variation, c_v, of each descriptor within periods during which $[K^+]$ levels remain nearly unchanged, but the signal quality was expected to vary. c_v was estimated for each patient as follows:

$$c_v = \frac{s}{\bar{x}}, \tag{11}$$

where s and $\bar{x}$ are the standard deviation and mean of either θ_δ or T_{SA} within a given period, respectively. Lower c_v values within periods of low signal quality indicate higher descriptor stability and, therefore, more robustness to noise.

Since ambulatory signals are recorded in an unsupervised fashion, c_v was measured in two different periods: t_1 = [21:00–22:00] of *Day 1* and t_2 = [00:00–01:00] of *Day 2*. During t_1, the patients were still awake, and the ECGs were expected to have lower quality due to movement (e.g., walking around the house). Conversely, during t_2, patients were asleep and physical activity was minimal, thereby increasing quality. We confirmed this through accelerometer signals recorded synchronously with the ECGs. The periods t_1 and t_2 were chosen for two reasons: (i) intra- and

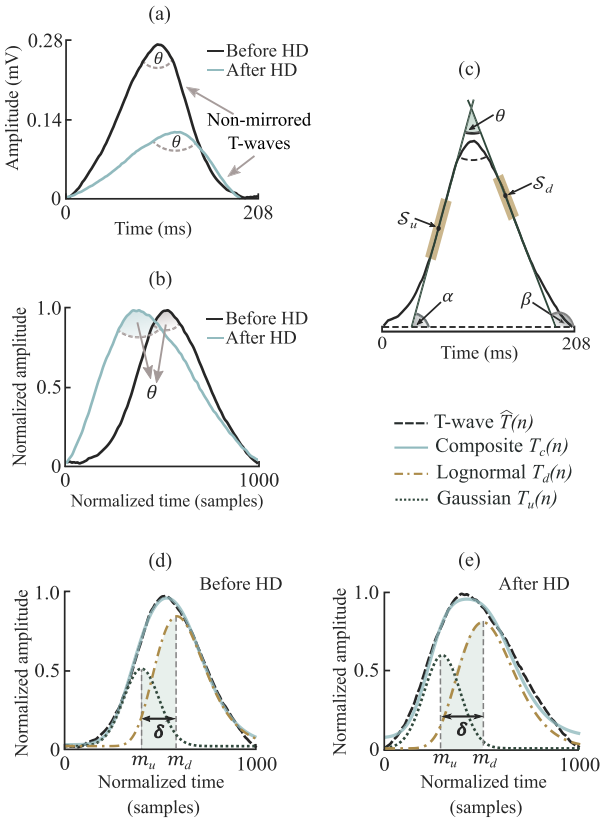

FIGURE 5. T-wave feature estimation: (a) T-waves before and after HD without normalization; (b) variation of θ in normalized T-waves before and after HD; (c) finding of $\mathcal{S}_u$, $\mathcal{S}_d$ and θ. The change in δ: (d) before HD ($[K^+] = 5.5$ mmol/L) and (e) after HD ($[K^+] = 3.2$ mmol/L).

intercellular $[K^+]$ changes are likely more stable during *Day 1* and *Day 2*, unlike during the same day after HD [33]; (ii) the circadian variability of serum $[K^+]$ in patients with impaired renal function indicates that $[K^+]$ levels between 21:00 till 01:00 increase, on average, only 0.06 mmol/L [34], which is minimal. Although the circadian variability of serum $[K^+]$ in HD patients has not been studied, we observed that θ_δ responded similarly to the findings in [34] (see Fig. 9), thus implying that the circadian rhythm is maintained.

III. RESULTS

Figure 6 depicts the variation of θ_δ and T_{SA} in patients of *Group I*. As expected, θ_δ and T_{SA} rise with the increase of $[K^+]$. Note the low trendline steepness for patient #6 which corresponds well with little change in $[K^+]$. Interestingly, T_{SA} varies in the opposite direction in patient #4 who displayed positive and negative T-waves, and occasional ST depression. θ_δ appears to better deal with alternating T-wave morphologies than T_{SA}.

Figure 7 shows the feature variation in patients of *Group II* of problematic recordings. Unsurprisingly, θ_δ and T_{SA} show trends discordant with $[K^+]$ levels in patients with: atrial fibrillation (#8), premature atrial contractions (#9), and tachycardia (#9, #10, #14). Nevertheless, in periods of sinus rhythm, during which the T-wave morphology stabilizes, both descriptors varies agreeably with $[K^+]$ levels.

Most of the time, flat or negative T-waves prevailed in patients #5 and #12, who manifested severe isolated hypocalcemia. T_{SA} could only be computed during the short time intervals in which the T-wave was positive. Curiously, both patients displayed discrepantly high θ_δ values despite the absence of hyperkalemia, likely due to T-wave narrowing during ST-T complex resampling used for correction of heart-rate induced T-wave changes.

In patients with hyperkalemia concomitant with metabolic acidosis (#10, #11, #13), T_{SA} showed a more prominent trendline steepness, possibly due to the overlaying effects of both electrolytes on the T-wave downward slope.

The daily distributions of $\theta_\delta - \theta_{\delta_{t0}}$ and $T_{SA} - T_{SA_{t0}}$ are given in Fig. 8. As anticipated, η responds inversely to $[K^+]$ variations, i.e., lower η values (patients #1–4, #8, and #12) indicate a higher increase in $[K^+]$ and, thus a smaller overlap of distributions, and vice-versa (patients #6, #10). The Pearson's correlation coefficient shows that both descriptors are moderately correlated with changes in $[K^+]$, being $r = -0.56$ ($p<0.01$) for θ_δ and $r = -0.57$ ($p<0.01$) for T_{SA}. When calculated for each group separately, the correlation is much stronger in *Group I* with $r = -0.81$ ($p>0.01$) for θ_δ and $r = -0.79$ ($p>0.01$) for T_{SA}, with *Group II* showing a weaker correlation of $r = -0.45$ ($p>0.01$) for θ_δ and $r = -0.44$ ($p>0.1$) for T_{SA}. It appears that θ_δ is more stable than T_{SA} except for #9, #14, and #15, for whom η_{0-2} show unexpected values compared to $\Delta[K^+]_{0-2}$. In patients who displayed both metabolic acidosis and hyperkalemia (#10, #11, and #13), T_{SA} shows lower η_{0-2} values for $\Delta[K^+]_{0-2}$. Broader distributions are observed in patients #4, #5, #9, #12, and #15 who exhibited T-wave morphologies across the long interdialytic interval different from those used to estimate $\theta_{\delta_{t0}}$ and $T_{SA_{t0}}$. A decrease of θ_δ and T_{SA} during *Day 0* is visible in the majority of patients, possibly due to insulin spikes during meals which can drive $[K^+]$ intracellularly.

Figure 9 shows the mean of θ_δ across all patients in non-overlapping 10 min intervals from 07:00 till 22:00. During *Day 1* and *Day 2*, θ_δ shows higher values in the morning, peaks around lunch time ([12:00-14:00]), and decreases across the afternoon until the evening. Also θ_δ increases during the night as θ_δ is higher at 07:00 of *Day 2* compared to 22:00 of *Day 1*.

Figure 10 shows the dispersion of c_v for θ_δ and T_{SA} within the periods of low (t_1) and high (t_2) signal quality. As envisaged, both descriptors show higher c_v values during t_1. However, θ_δ displays lower dispersion of c_v during t_1, suggesting greater stability in noisy conditions than T_{SA}. While the median difference of T_{SA} is minimal between t_1 and t_2, T_{SA} exhibits a large dispersion during t_2. In contrast, θ_δ seems to be more constant in less noisy conditions. Patients #8 and #12 were excluded from this analysis as #12 displayed T-wave inversion (for which T_{SA} cannot be estimated) and #8 manifested atrial fibrillation during t_1 and t_2.

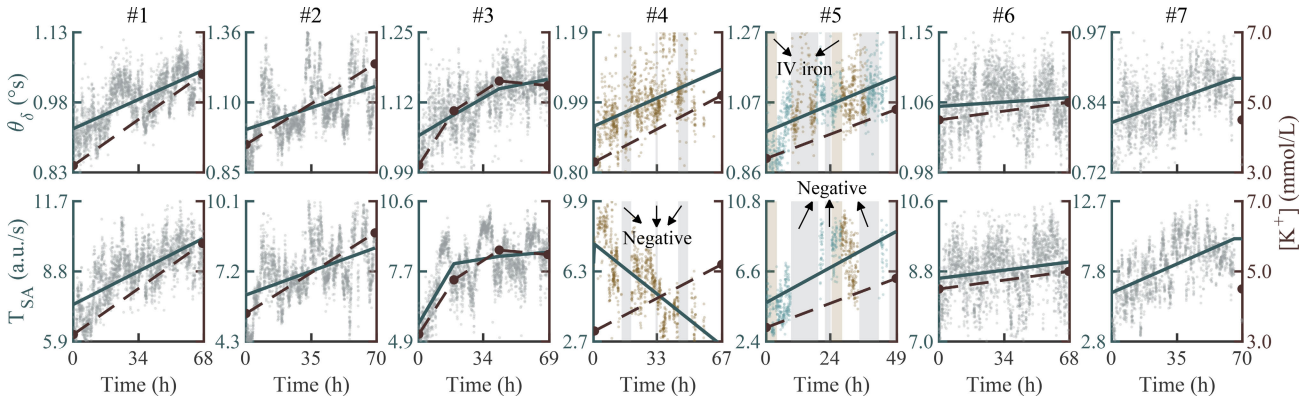

FIGURE 6. Variation of θ_δ (top row) and T_{SA} (bottom row) together with the estimated linear trend (solid blue line) and [K$^+$] values (red dots, dashed line) for individual patients of *Group I*. The linear trends are estimated using the best-fit linear polynomial between the consecutive time instances of [K$^+$] assessments. Grey patches depict periods of negative T-waves, during which θ_δ is computed without any correspondent T_{SA} values. Yellow patches depict periods of intravenous (IV) iron infusion which may affect T-wave morphology. Patient #5 was taken to HD one day earlier and, thus no blood was taken between HD sessions. The blood samples from Friday HD of patient #7 were misplaced hence the absent trendline. Dots of different colors highlight patients who displayed metabolic acidosis (yellow) or severe hypocalcemia and metabolic acidosis (blue and yellow).

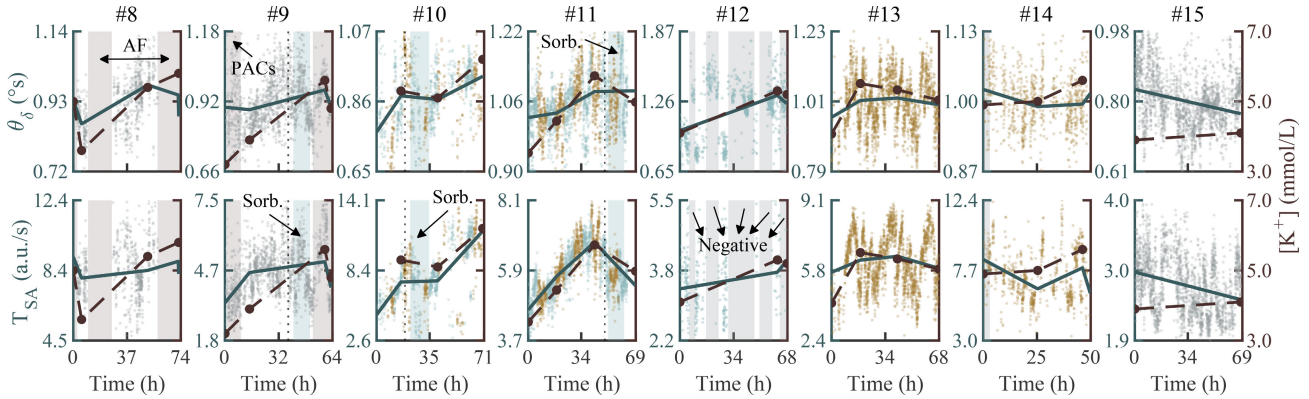

FIGURE 7. Variation of θ_δ (top row) and T_{SA} (bottom row) together with the estimated linear trend (solid blue line) and [K$^+$] values (red dots, dashed line) for individual patients of *Group II*. The linear trends are estimated using the best-fit linear polynomial between the consecutive time instances of [K$^+$] assessments. Grey patches depict periods of negative T-waves, during which θ_δ is computed without any correspondent T_{SA} values. Red patches depict periods of arrhythmias: atrial fibrillation (AF) and premature atrial contractions (PACs). Patient #14 was taken to HD one day earlier. The blood sample at the end of Friday HD of patient #10 was misplaced. Dashed vertical line denotes the time of Sorbisterit (Sorb) intake, whereas blue patches depict the duration of Sorbisterit effect. Dots of different colors highlight patients who displayed metabolic acidosis (yellow), severe hypocalcemia (blue) or both.

IV. DISCUSSION

A. DESCRIPTORS RESPONSIVENESS TO POTASSIUM FLUCTUATIONS

We quantified gradual electrolyte-induced T-wave changes using model-based parametrization. The yielded parameters of such models can act as surrogates of important physiological traits that cannot be straightforwardly determined (e.g., T-wave duration) [35]. Additionally, model-based parametrization enables a global evaluation of the T-wave morphology and may increase robustness to noise [36], which is frequent in ambulatory ECG recordings. We tracked T-wave morphology changes using two descriptors: θ_δ, and T_{SA}. The progression of θ_δ and T_{SA} during the long interdialytic interval is promising, both showing an appealing potential to become estimators of serum [K$^+$]. Even in a group of patients with various underlying cardiac diseases, θ_δ and T_{SA} are responsive to [K$^+$] fluctuations, indicating that long-term monitoring of such fluctuations is feasible. Furthermore, θ_δ exhibited higher stability during noisy periods compared to T_{SA}, which is advantageous for ambulatory monitoring.

Interestingly, the descriptors showed increased variability during *Day 0* compared to *Day 1* or *Day 2*. The presence of such variability is plausible since the effects of HD-induced hemodynamic stress could, presumably, still be felt for hours after HD, thus affecting T-wave morphology. The existence of such a transient period, during which the T-wave morphology can differ from the one manifested during the long interdialytic interval, may have substantial implications on [K$^+$] estimation. One approach for ECG-based estimation of [K$^+$] levels can be the use of a reference T-wave of each individual at a known [K$^+$] level. Indeed, previous studies have shown a decrease in the error of [K$^+$] estimation after patient-specific calibration [13], [15]. However, these

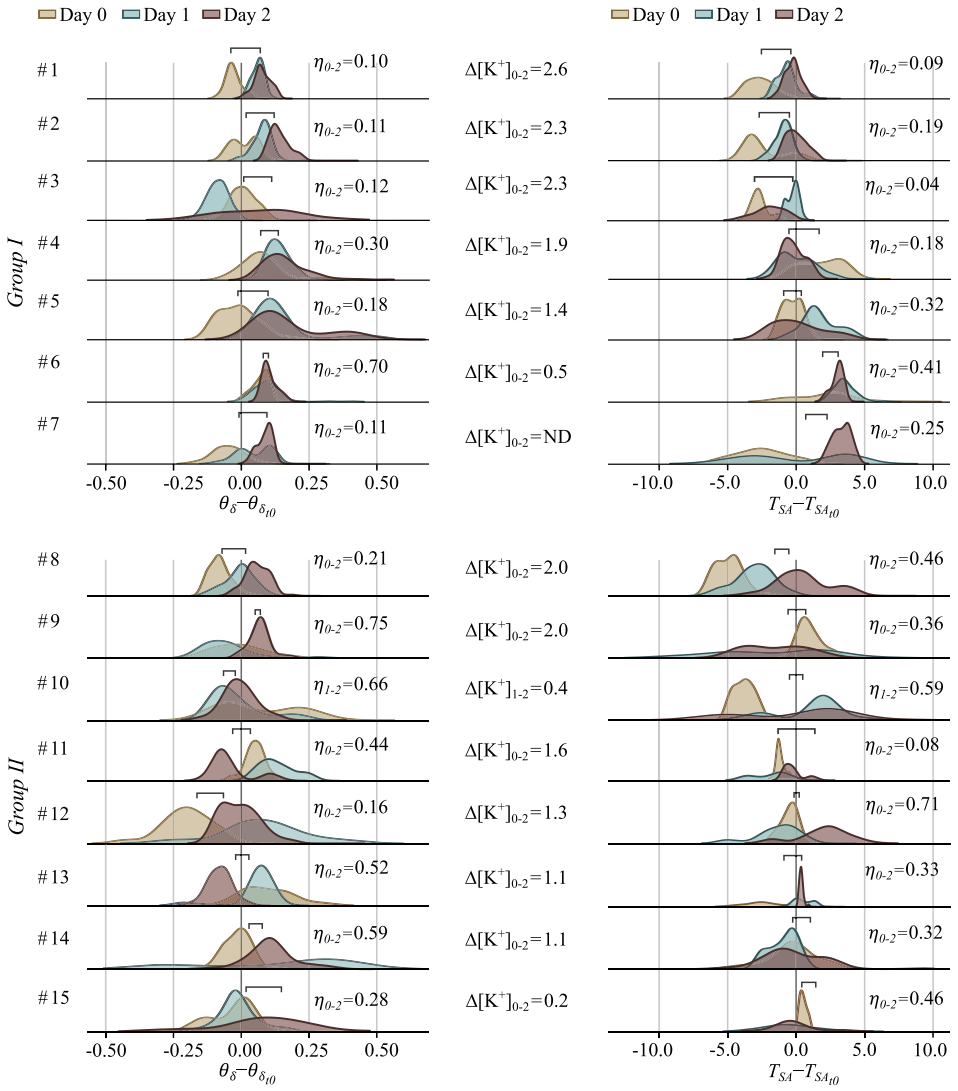

FIGURE 8. Distribution of $\theta_\delta - \theta_{\delta_{t0}}$ (left) and $T_{SA} - T_{SA_{t0}}$ (right) of *Group I* (top) and *Group II* (bottom) during the long interdialytic interval. η_{0-2} is the overlapping index between the distributions of *Day 0* and *Day 2*, whereas $\Delta[K^+]_{0-2}$ is the increment of $[K^+]$ between the end of Friday HD and the start of Monday HD. The number of intervals during *Day 2* is small in patients #5 and #14 who were taken to HD one day earlier. The blood samples from Friday HD of patients #7 and #10 were misplaced (ND stands for no data). In patient #10, blood was collected on *Day 1*.

studies focused on assessing $[K^+]$ levels during HD exclusively, where the same T-wave morphology—similar to that used to estimate reference values—persists throughout HD. Using T-waves acquired during or immediately after HD as a reference may result in $[K^+]$ estimation errors when the morphology alters. Thus, days between HD sessions should preferably be used for reference T-wave assessment.

Another finding is the apparent circadian periodicity of θ_δ, suggesting that $[K^+]$ naturally fluctuates during the day in HD patients similarly to healthy subjects [34]. Although there is a lack of studies examining the circadian rhythm of serum $[K^+]$ levels in HD patients, the existence of such circadian variability in these patients is still plausible. With little to no renal function left, as an attempt to maintain $[K^+]$ homeostasis, HD patients heavily rely on aldosterone-regulated colonic $[K^+]$ secretion [37], [38]. While the circadian rhythm of aldosterone is well understood in healthy subjects [39], it is unclear whether HD patients maintain such circadian rhythm.

Our study showed that θ_δ and T_{SA} started to decrease 2 h after the intake of potassium-lowering medication (Sorbisterit), which is compatible with its onset of action. The decrease of θ_δ and T_{SA} lasted about 10 h and is within the range of expected duration of the Sorbisterit effect. This observation needs to be taken into account to understand better how Sorbisterit, or other standard medications prescribed to HD patients, alters the T-wave morphology.

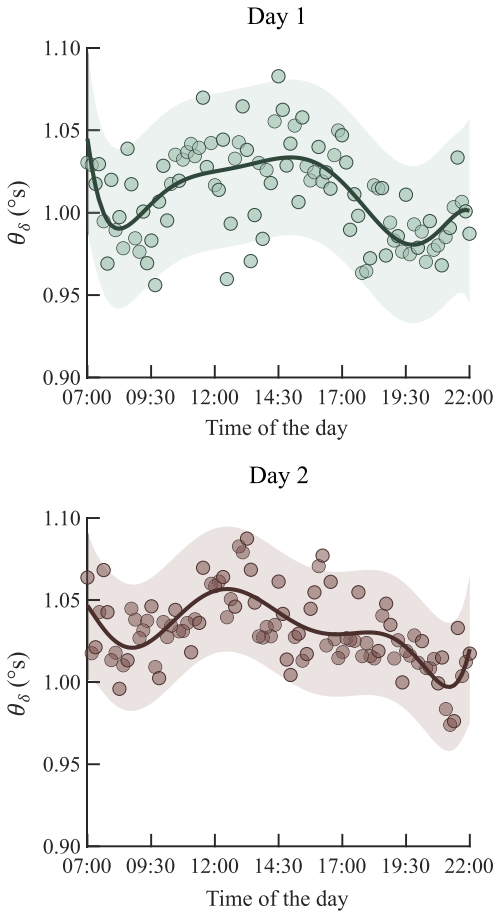

FIGURE 9. Mean of θ_δ (dots) across all patients in non-overlapping 10 intervals from 07:00 till 22:00 during *Day 1* and *Day 2*. Solid line is a fitted 7^{th} order polynomial to show a smoother variation of θ_δ. The upper and lower boundaries represent the standard deviation of the fitted polynomial.

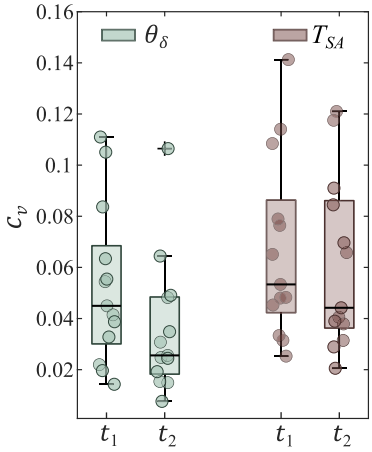

FIGURE 10. Boxplot of coefficient of variation c_v computed for each patient during two different signal quality periods: t_1 = [21:00–22:00] of *Day 1* (lower signal quality) and t_2 = [00:00–01:00] of *Day 2* (higher signal quality).

B. EVALUATION OF SERUM POTASSIUM WITH CONCURRENT CALCIUM IMBALANCE

Compared to T_{SA}, the range of θ_δ values is narrower and more consistent across the dataset, except for patients with isolated severe hypocalcemia (#5 and #12), both free from any pre-existent cardiac issues. Intriguingly, these patients exhibited high θ_δ values without hyperkalemia. We found atypically low values of δ in these patients, which indicate T-wave narrowing as, conceptually, δ mostly depends on T-wave duration. Considering that the T-wave duration is not affected by calcium imbalance with normal $[K^+]$ levels [9], δ should not have reacted in this manner. We suspect that resampling of the ST-T complex, distinctively prolonged in hypocalcemia [9], may have affected the T-wave duration.

While flattened or negative T-waves can be prominent in isolated calcium abnormalities [9], [40], particularly in severe levels, changes in ST-segment duration are the most discernible marker of [Ca] levels [9]. Although this study did not analyze in detail the effects of [Ca] on the ECG, we observed a prolonged ST-segment in three patients who displayed severe hypocalcemia. However, ambulatory estimation of the ST-segment duration is challenging, particularly in pathological conditions of ST-segment deviations, as frequently encountered in HD patients. For instance, in patient #10 with ST-elevation characteristic of left ventricular hypertrophy (LVH), the ST-elongation was not as blatant in lead-I as in patients #5 and #12, both without ST-deviations. Perhaps in cases of ST-segment deviations, relying on other ECG leads can mitigate this problem.

Recognizing abnormal calcium levels may improve the detection of dangerous serum $[K^+]$ levels for twofold reasons. Firstly, isolated calcium imbalance can alter the T-wave morphology [9], thus interfering with the assessment of potassium-induced T-wave changes. Secondly, [Ca] and $[K^+]$ have a complex relationship which affects the intra- and atrioventricular conduction within the heart [9], meaning that the harmfulness of $[K^+]$ levels, either in hypo- or hyperkalemia, is tightly dependent on [Ca] levels [7]. For instance, hypercalcemia antagonizes, whereas hypocalcemia exacerbates the consequences of hyperkalemia [21]. Determining the presence of calcium imbalance can aid in ascertaining whether the measured $[K^+]$ level is alarming or not.

C. EVALUATION OF SERUM POTASSIUM WITH CONCURRENT ACID-BASE IMBALANCE

Along with concurrent calcium imbalance, we also encountered difficulties in detecting $[K^+]$ fluctuations in the presence of an acid-base disturbance (i.e., abnormal $[HCO_3^-]$ levels). When acidosis emerges, the electrophysiological effects of hyperkalemia are, expectedly, aggravated [21]. Consequently, one would anticipate θ_δ and T_{SA} to respond with higher values in such conditions, which was not entirely the case in patients with hyperkalemia and acidosis. Curiously, though rare, severe hyperkalemia with minimal T-wave changes has been reported in patients who manifested acidosis concurrently [41]. Although noisy recordings or LVH could reasonably justify such an unexpected variation of θ_δ and T_{SA}, the impact of acidosis in $[K^+]$ estimation should not be neglected. Acidosis can instigate T-wave morphology changes resembling those of hyperkalemia [42]. Using solely

T-wave-derived features to evaluate $[K^+]$ levels when acidosis arises, may, therefore, either under- or overestimate $[K^+]$ levels.

A compelling case to mention is patient #15, whose values of θ_δ and T_{SA} decreased during the long interdialytic interval. Besides being the patient with the most complicated medical history, including chronic heart failure, LVH, and ischemic heart disease, he was the only patient who experienced metabolic alkalosis. Even though alkalosis does not usually cause hypokalemia in HD patients [43], it is peculiar to see that θ_δ and T_{SA} decreased. Such behavior of θ_δ and T_{SA} is something we would expect in case of $[K^+]$ depletion as in hypokalemia. Since alkalosis-related ECG changes resemble those of hypokalemia [44], one must pose the question of whether this unusual descriptor variation results, inherently, from the heart failure condition, or as a consequence of alkalosis.

While blood pH imbalance is seldom life-threatening in itself if not in severe levels [45], identifying acid-base disturbances may not only improve $[K^+]$ monitoring but also aid in assessing the arrhythmogenic potential of $[K^+]$. In addition to being vastly prevalent in HD patients, acid-base disequilibrium can encourage the onset of arrhythmias by (i) impairing vascular and myocardial function [46], and (ii) influencing the levels of various electrolytes, including $[K^+]$, [Na], and [Ca] [42], [45]. For instance, metabolic acidosis induces $[K^+]$ shifts from the intracellular to the extracellular space, potentially leading to hyperkalemia [45]. Thus, identifying $[HCO_3^-]$ imbalance could enable better management of serum $[K^+]$. Nevertheless, with $[K^+]$ and $[HCO_3^-]$ compounding their effects on the T-wave morphology, the feasibility of utilizing a single-lead ECG to monitor $[K^+]$ fluctuations in the presence of abnormal $[HCO_3^-]$ levels is, at the very least, contentious. Future studies should address the confounding potential of $[HCO_3^-]$ by exploring other descriptors of $[HCO_3^-]$ levels.

D. CHALLENGES AND LIMITATIONS

Even with encouraging results, deriving θ_δ and T_{SA} in ambulatory conditions still poses some obstacles to be tackled, one of them being the inherent complexity of determining T-wave boundaries in noisy conditions. When tachycardia or an episode of premature atrial contractions (PACs) occur, the P-wave can partially hide within the preceding T-wave, resulting in either a disturbed T-wave morphology or a misguided delineation of the T-wave. We experienced difficulties in accurately locating T-waves during tachycardia or PAC episodes. Even though employing a SQI detector should have disregarded ECG segments with premature heartbeats, the SQI used in this work failed to identify PAC episodes, eliminating exclusively ventricular ectopic beats and noisy segments. Premature heartbeats, atrial or ventricular, must be detected not only to avoid erroneously locating the T-wave but also because alterations in serum $[K^+]$ and $[Mg^{2+}]$ can trigger ectopy and, consequently, arrhythmias [8]. The frequency of ectopy occurrence might, therefore, be an indicator of electrolyte fluctuations.

Alternating T-wave morphologies is another issue deserving further exploration. Independently of whether different physiological conditions instigate morphology variations, the disparity in observed T-wave morphologies, even in the same patient, further demonstrates the importance of dealing with various T-wave morphologies. With previous studies having used, exclusively, intradialytic T-waves to seed models for quantification of serum $[K^+]$, the performance of such models is, arguably, fettered when encountering different interdialytic morphologies. While estimating $[K^+]$ levels from T-waves identical to the patient-specific reference is ideal, it may not always be attainable to do so during activities of daily living. Availability of multiple ECG leads and lead-reduction techniques could ameliorate the problem of alternating T-wave morphologies [47]; however, 12-lead ECG recorders are often uncomfortable for wearing and hence unsuitable for long-term monitoring. Handling various ECG morphologies is, therefore, indispensable for noninvasive monitoring of electrolyte fluctuations. Indeed, in a highly susceptible group of HD patients, the discrepancy in T-wave morphologies can stem from many sources, either psychological stress [48], change in body position [23], physical activity [49], other electrolyte imbalances [9], or due to pre-existent cardiac comorbidities. Understanding the causes of morphology changes in HD patients is pivotal to avoid misclassification of other pathologies and electrolyte imbalance.

The small number of patients included in this study, albeit being a realistic representation of the HD population, certainly restricts the generalization of our findings, especially to other populations susceptible to $[K^+]$ imbalance. Furthermore, the lack of patients with severe hypo- or hyperkalemia prevents us from evaluating the descriptor response in such extreme cases with distinct ECG morphology.

The exploration of additional electrolyte biomarkers is needed. Having biomarkers of serum $[K^+]$, [Ca], and $[HCO_3^-]$ can facilitate routine electrolyte monitoring, aid in ascertaining the harmfulness of $[K^+]$ levels, and possibly avert life-threatening conditions. Thus, our future studies will focus on developing descriptors of [Ca] and $[HCO_3^-]$ levels and optimize $[K^+]$ estimation under concomitant electrolyte imbalance. Future studies should also strive to collect blood samples on days between HD sessions and extend to other patient populations susceptible to $[K^+]$ imbalance (e.g., heart failure).

To the best of our knowledge, this is the first study to attempt to monitor gradual $[K^+]$ fluctuations throughout the long interdialytic interval, thereby narrowing any possibility to compare our findings. Nevertheless, we reveal the central issues to be solved concerning the noninvasive monitoring of electrolyte fluctuations in HD patients.

V. CONCLUSION

This study demonstrates that long-term noninvasive monitoring of $[K^+]$ fluctuations is feasible even in complicated

HD patients with underlying cardiac diseases. Given the preponderance of alternating T-wave morphologies that can differ from the one exhibited during HD within the same patient, reference T-waves should preferably be assessed in days between HD sessions.

Gradual T-wave morphology changes induced by serum $[K^+]$ can be quantified by model-based parametrization (θ_μ) and slope-to-amplitude ratio (T_{SA}). θ_μ appears to be less affected by noise than T_{SA}, and, therefore better suited for long-term monitoring during daily activities. However, the presence of concomitant electrolyte imbalance, primarily of [Ca] and $[HCO_3^-]$, can hamper a reliable estimation of $[K^+]$ levels and should be accounted for.

APPENDIX A
INITIALIZATION OF THE FITTING ALGORITHM

The lower and upper boundaries, and initial values of the elements of vector $\boldsymbol{\phi}$ are presented in Table 2. These values

Algorithm 1 T-Wave Rectification

Input: Delineated T-wave $T(n)$
Output: Rectified T-wave $T(n)$, standardized T-wave $T^z(n)$, T-wave waverform *type*

procedure TwaveRectification($T(n)$)
  $T(n) \leftarrow []$
  $T^z(n) \leftarrow []$
  type ← Check type of $T(n)$. See Figure 4.
  if *type*! = *flat* **then**
    if *type* == *negative* **then**
      $T(n) \leftarrow -T(n)$ ▷ Invert $T(n)$
    else if *type* == *ST depression* **then**
      iOnset ← Find local minima index of $T(n)$.
      $T(n) \leftarrow T(iOnset{:}n)$ ▷ Amend T-wave onset
    end if
    $T(n) \leftarrow$CorrectBaseline($T(n)$)
    $T^z(n) \leftarrow$TwaveStandardization($T(n)$)
  end if
  return $T(n)$, $T^z(n)$, *type*
end procedure

procedure CorrectBaseline($T(n)$)
  baseline ← Linear interpolation between $T(n)$ onset and offset.
  $T(n) \leftarrow T(n) - baseline$
  return $T(n)$
end procedure

procedure TwaveStandardization($T(n)$)
  $\bar{x} \leftarrow mean(T(n))$
  $s \leftarrow std(T(n))$
  $T^z(n) \leftarrow \frac{T(n)-\bar{x}}{s}, \forall n$. See (1).
  return $T^z(n)$
end procedure

Algorithm 2 T-Wave Parametrization

Input: Baseline-removed T-wave $T(n)$
Output: Parameters σ_d, μ_u, μ_d, γ_d, and R^2

procedure TwaveParametrization($T(n)$)
  $T(n) \leftarrow$ resample $T(n)$ to 1000 samples.
  $T(n) \leftarrow$ normalize $T(n)$ to unit amplitude.
  $\widehat{T}(n) \leftarrow T(-n)$ ▷ Mirroring
  $N \leftarrow length(T(n))$
  $T_c^i(n; \boldsymbol{\phi_i}) \leftarrow$GetIntitialTemplate($\widehat{T}(n)$, N)
  $T_c(n; \boldsymbol{\phi}), R^2 \leftarrow$LScurveFit($T_c^i(n; \boldsymbol{\phi_i})$)
  $\sigma_d, \mu_u, \mu_d, \gamma_d \leftarrow$ extract from $\boldsymbol{\phi}$
  return $\sigma_d, \mu_u, \mu_d, \gamma_d, R^2$
end procedure

procedure GetInitialTemplate($\widehat{T}(n)$, N)
  $b \leftarrow \frac{N}{1000}$
  $n_p \leftarrow$ find $\widehat{T}(n)$ peak sample location
  Use b, n_p, and Table 2 to initialize $\boldsymbol{\phi_i}$.
  $\boldsymbol{\phi_i} \leftarrow [\sigma_u, \sigma_d, \mu_u, \mu_d, \gamma_d, w_u, w_d, h]$.
  $n \leftarrow [0{:}length(\widehat{T}(n))-1]$
  $T_u^i(n; \sigma_u, \mu_u) \leftarrow$ construe Gaussian as in (2).
  $T_d^i(n; \sigma_d, \mu_d, \gamma_d) \leftarrow$ construe Lognormal as in (3).
  $T_c^i(n; \boldsymbol{\phi_i}) \leftarrow w_u T_u^i(x) + w_d T_d^i(x) + h$. See (4).
  return $T_c^i(n; \boldsymbol{\phi_i})$
end procedure

procedure LScurveFit($T_c^i(n; \boldsymbol{\phi_i})$)
  $\boldsymbol{\phi_{low}} \leftarrow$ lower boundaries. See Table 2.
  $\boldsymbol{\phi_{up}} \leftarrow$ upper boundaries. See Table 2.
  $T_c(n; \boldsymbol{\phi}) \leftarrow$ Trust-region reflective least-squares algorithm with the given boundaries.
  $R^2 \leftarrow$ calculate coefficient of determination.
  return $T_c(n; \boldsymbol{\phi}), R^2$
end procedure

TABLE 2. Initial values, lower and upper boundaries used to estimate the elements of $\boldsymbol{\phi}$.

	$T_u(n)$			$T_d(n)$				
Elements of $\boldsymbol{\phi}$	σ_u	μ_u	w_u	σ_d	μ_d	γ_d	w_d	h
Initial value	10.9	n_p	3.1	0.52	$0.2(\ln b)$	n_p	4.1	0.2
Lower boundary	$7.7b$	$0.25n_p$	25	$0.01(b \ln b)$	$0.4(\ln b)$	−90	142	−2.0
Upper boundary	$9.7b$	$0.9n_p$	129	$0.035(b \ln b)$	$8.8(\ln b)$	900	286	3.0

Algorithm 3 Feature Estimation

Input: Delineated $T(n)$
Output: θ_δ, T_{SA}

$T_o(n) \leftarrow T(n)$
$T(n), T^z(n), type \leftarrow$TwaveRectification$T(n)$
if $type! = flat$ **then**
    $\mathcal{S}_u$, $\mathcal{S}_d$ $\leftarrow$ Estimate T-wave slopes from $T^z(n)$ as in [30].
    $\theta_\delta \leftarrow$EstimateThetaDelta$(T(n), \mathcal{S}_u, \mathcal{S}_d)$
    if $type! = negative$ **then**
        T_{SA} $\leftarrow$ Estimate T_{SA} from $T_o(n)$ as described in [15].
    else
        $T_{SA} \leftarrow []$
    end if
end if

procedure EstimateThetaDelta$(T(n), \mathcal{S}_u, \mathcal{S}_d)$
    $\theta_\delta \leftarrow []$
    $N \leftarrow length(T(n))$
    $\sigma_d, \mu_u, \mu_d, \gamma_d, R^2 \leftarrow$TwaveParametrization$(T(n))$
    if $R^2 \geq 0.8$ **then**
        $\theta \leftarrow \arctan(\mathcal{S}_d) - \arctan(\mathcal{S}_u)$
        $m_u \leftarrow \mu_u$
        $m_d \leftarrow \gamma_d + e^{(\mu_d - \sigma_d^2)}$
        $\widehat{\delta} \leftarrow m_d - m_u$
        $\delta \leftarrow \widehat{\delta}\frac{N}{1000}$
        $\theta_\delta \leftarrow -\log_{10}(\theta \cdot \delta)$
    end if
    return θ_δ
end procedure

were determined empirically and are dependent on $T(n)$ and $\widehat{T}(n)$. In the table, n_p denotes the T-wave peak sample location of $\widehat{T}(n)$, whereas $b = \frac{N}{1000}$, where N is the number of samples in $T(n)$.

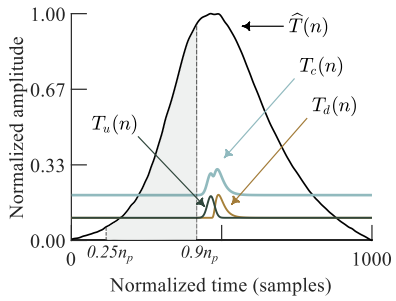

FIGURE 11. Template for initialization of the fitting algorithm.

The initial values of $\boldsymbol{\phi}$ can be modified as long as the initial template is similar to the one shown in Fig. 11. The composite $T_c(n)$ must be beneath $\widehat{T}(n)$ peak. The location parameter μ_u ensures that $T_u(n)$ always fits the upward slope, thus the lower and upper boundaries of μ_u depend on the peak location. The boundaries guarantee $T_u(n)$ is centered within [25%—90%] of the upward portion of $\widehat{T}(n)$ as shown in Fig 11. The scale parameter μ_d evaluates how ''shrunk'' or ''stretched'' the T-wave is. Accordingly, $\ln b$ is used to better adapt the algorithm to different T-waves.

APPENDIX B
PSEUCODE OF THE DEVELOPED ALGORITHM

T-wave rectification steps are described in Algorithm 1, T-wave parametrization in Algorithm 2. Algorithm 3 explains the procedure for feature estimation.

REFERENCES

[1] M. C. G. Wong, J. M. Kalman, E. Pedagogos, N. Toussaint, J. K. Vohra, P. B. Sparks, P. Sanders, P. M. Kistler, K. Halloran, G. Lee, S. A. Joseph, and J. B. Morton, ''Temporal distribution of arrhythmic events in chronic kidney disease: Highest incidence in the long interdialytic period,'' *Heart Rhythm*, vol. 12, no. 10, pp. 2047–2055, Oct. 2015.
[2] S. Genovesi, G. Boriani, A. Covic, R. W. M. Vernooij, C. Combe, A. Burlacu, A. Davenport, M. Kanbay, D. Kirmizis, D. Schneditz, F. van der Sande, and C. Basile, ''Sudden cardiac death in dialysis patients: Different causes and management strategies,'' *Nephrol. Dialysis Transplantation*, vol. gfz182, pp. 1–10, Sep. 2019, doi: 10.1093/ndt/gfz182.
[3] J. Perl and C. T. Chan, ''Timing of sudden death relative to the hemodialysis procedure,'' *Nature Clin. Pract. Nephrol.*, vol. 2, no. 12, pp. 668–669, Dec. 2006.
[4] M. P. Turakhia, P. J. Blankestijn, J. J. Carrero, C. M. Clase, R. Deo, C. A. Herzog, S. E. Kasner, R. S. Passman, R. Pecoits-Filho, H. Reinecke, and G. R. Shroff, ''Chronic kidney disease and arrhythmias: Conclusions from a kidney disease: Improving global outcomes (KDIGO) controversies conference,'' *Eur. Heart J.*, vol. 39, no. 24, pp. 2314–2325, 2018.
[5] A. Welch, N. Maroz, and C. S. Wingo, ''Hyperkalemia: Getting to the heart of the matter,'' *Nephrol. Dialysis Transplantation*, vol. 28, no. 1, pp. 15–16, Jan. 2013.
[6] J. P. Kooman, F. P. Wieringa, M. Han, S. Chaudhuri, F. M. van der Sande, L. A. Usvyat, and P. Kotanko, ''Wearable health devices and personal area networks: Can they improve outcomes in haemodialysis patients?'' *Nephrol. Dialysis Transplantation*, vol. 35, no. 2, pp. 1143–1150, Mar. 2020.
[7] N. El-Sherif and G. Turitto, ''Electrolyte disorders and arrhythmogenesis,'' *Cardiol. J.*, vol. 18, no. 3, p. 13, 2011.
[8] J. N. Weiss, Z. Qu, and K. Shivkumar, ''Electrophysiology of hypokalemia and hyperkalemia,'' *Circulat., Arrhythmia Electrophysiol.*, vol. 10, no. 3, Mar. 2017, Art. no. e004667.
[9] B. Surawicz, ''Relationship between electrocardiogram and electrolytes,'' *Amer. Heart J.*, vol. 73, no. 6, pp. 814–834, Jun. 1967.
[10] K. D. Wrenn, C. M. Slovis, and B. S. Slovis, ''The ability of physicians to predict hyperkalemia from the ECG,'' *Ann. Emergency Med.*, vol. 20, no. 11, pp. 1229–1232, Nov. 1991.
[11] B. T. Montague, J. R. Ouellette, and G. K. Buller, ''Retrospective review of the frequency of ECG changes in hyperkalemia,'' *Clin. J. Amer. Soc. Nephrology*, vol. 3, no. 2, pp. 324–330, Mar. 2008.
[12] N. Durfey, B. Lehnhof, A. Bergeson, S. Durfey, V. Leytin, K. McAteer, E. Schwam, and J. Valiquet, ''Severe hyperkalemia: Can the electrocardiogram risk stratify for short-term adverse events?'' *Western J. Emergency Med.*, vol. 18, no. 5, pp. 963–971, Aug. 2017.
[13] C. Corsi, M. Cortesi, G. Callisesi, J. De Bie, C. Napolitano, A. Santoro, D. Mortara, and S. Severi, ''Noninvasive quantification of blood potassium concentration from ECG in hemodialysis patients,'' *Sci. Rep.*, vol. 7, no. 1, pp. 1–10, Mar. 2017.
[14] J. J. Dillon, C. V. DeSimone, Y. Sapir, V. K. Somers, J. L. Dugan, C. J. Bruce, M. J. Ackerman, S. J. Asirvatham, B. L. Striemer, J. Bukartyk, C. G. Scott, K. E. Bennet, S. B. Mikell, D. J. Ladewig, E. J. Gilles, A. Geva, D. Sadot, and P. A. Friedman, ''Noninvasive potassium determination using a mathematically processed ECG: Proof of concept for a novel 'blood-less, blood test,''' *J. Electrocardiol.*, vol. 48, no. 1, pp. 12–18, Jan. 2015.
[15] Z. I. Attia, C. V. DeSimone, J. J. Dillon, Y. Sapir, V. K. Somers, J. L. Dugan, C. J. Bruce, M. J. Ackerman, S. J. Asirvatham, B. L. Striemer, J. Bukartyk, C. G. Scott, K. E. Bennet, D. J. Ladewig, E. J. Gilles, D. Sadot, A. B. Geva, and P. A. Friedman, ''Novel bloodless potassium determination using a signal-processed single-lead ECG,'' *J. Amer. Heart Assoc.*, vol. 5, no. 1, Jan. 2016.

[16] O. Z. Yasin, Z. Attia, J. J. Dillon, C. V. DeSimone, Y. Sapir, J. Dugan, V. K. Somers, M. J. Ackerman, S. J. Asirvatham, C. G. Scott, K. E. Bennet, D. J. Ladewig, D. Sadot, A. B. Geva, and P. A. Friedman, "Noninvasive blood potassium measurement using signal-processed, single-lead ecg acquired from a handheld smartphone," *J. Electrocardiol.*, vol. 50, no. 5, pp. 620–625, Sep. 2017.
[17] F. Palmieri, P. Gomis, J. E. Ruiz, B. Bergasa, F. Dina, A. Martin, S. H. Ahamed, E. Pueyo, J. P. Martínez, J. Ramírez, and P. Laguna, "T-wave morphology changes as surrogate for blood potassium concentration in hemodialysis patients," in *Proc. Comput. Cardiol. Conf. (CinC)*, Dec. 2019, p. 1.
[18] S. Hassaan Ahmed Bukhari, F. Palmieri, D. Ferreira, M. Potse, J. Ramírez, P. Laguna, C. Sanchez, and E. Pueyo, "Transmural ventricular heterogeneities play a major role in determining T-Wave morphology at different extracellular potassium levels," in *Proc. Comput. Cardiology Conf. (CinC)*, Dec. 2019.
[19] L. M. Einhorn, M. Zhan, V. D. Hsu, L. D. Walker, M. F. Moen, S. L. Seliger, M. R. Weir, and J. C. Fink, "The frequency of hyperkalemia and its significance in chronic kidney disease," *Arch. Internal Med.*, vol. 169, no. 12, p. 1156, Jun. 2009.
[20] B. Surawicz, H. Chlebus, and A. Mazzoleni, "Hemodynamic and electrocardiographic effects of hyperpotassemia. Differences in response to slow and rapid increases in concentration of plasma k," *Amer. Heart J.*, vol. 73, no. 5, pp. 647–664, May 1967.
[21] L. S. Weisberg, "Management of severe hyperkalemia," *Crit. Care Med.*, vol. 36, no. 12, pp. 3246–3251, Dec. 2008.
[22] C. Orphanidou, T. Bonnici, P. Charlton, D. Clifton, D. Vallance, and L. Tarassenko, "Signal-quality indices for the electrocardiogram and photoplethysmogram: Derivation and applications to wireless monitoring," *IEEE J. Biomed. Health Informat.*, vol. 19, no. 3, pp. 832–838, May 2015.
[23] M. G. Adams and B. J. Drew, "Body position effects on the ECG," *J. Electrocardiol.*, vol. 30, no. 4, pp. 285–291, Oct. 1997.
[24] B. Vandenberk, E. Vandael, T. Robyns, J. Vandenberghe, C. Garweg, V. Foulon, J. Ector, and R. Willems, "Which QT correction formulae to use for QT monitoring?" *J. Amer. Heart Assoc.*, vol. 5, no. 6, 2016.
[25] A. J. Demski and M. L. Soria, "ECG-kit: A MATLAB toolbox for cardiovascular signal processing," *J. Open Res. Softw.*, vol. 4, no. 1, pp. 2–4, 2016.
[26] C. R. Vázquez-Seisdedos, J. Neto, E. J. M. Reyes, A. Klautau, and R. C. Limão de Oliveira, "New approach for T-wave end detection on electrocardiogram: Performance in noisy conditions," *Biomed. Eng. OnLine*, vol. 10, no. 1, p. 77, 2011.
[27] A. Sološenko, A. Petrėnas, V. Marozas, and L. Sörnmo, "Modeling of the photoplethysmogram during atrial fibrillation," *Comput. Biol. Med.*, vol. 81, pp. 130–138, Feb. 2017.
[28] K. M. M. Huotari, A. Vehkaoja, and J. Kostamovaara, "Photoplethysmography and its detailed pulse waveform analysis for arterial stiffness," *J. Structural Mech.*, vol. 22, no. 4, pp. 345–362, 2011.
[29] A. Rodrigues, A. Petrėnas, N. Kušleikaitė-Pere, P. Laguna, and V. Marozas, "ECG-based monitoring of electrolyte fluctuations during the long interdialytic interval," in *Proc. Comput. Cardiol. Conf. (CinC)*, Dec. 2018, pp. 1–4.
[30] D. Romero, M. Ringborn, P. Laguna, and E. Pueyo, "Detection and quantification of acute myocardial ischemia by morphologic evaluation of QRS changes by an angle-based method," *J. Electrocardiol.*, vol. 46, no. 3, pp. 204–214, May 2013.
[31] T. J. Schaefer and R. W. Wolford, "Disorders of potassium," *Emergency Med. Clinics North Amer.*, vol. 23, no. 3, pp. 723–747, Aug. 2005.
[32] M. Pastore and A. Calcagnì, "Measuring distribution similarities between samples: A distribution-free overlapping index," *Frontiers Psychol.*, vol. 10, p. 1089, May 2019.
[33] A. Blumberg, H. Roser, C. Zehnder, and J. Müller-Brand, "Plasma potassium in patients with terminal renal failure during and after haemodialysis; relationship with dialytic potassium removal and total body potassium," *Nephrol. Dialysis Transplantation*, vol. 12, no. 8, pp. 1629–1634, Aug. 1997.
[34] S. T. Schmidt, T. Ditting, B. Deutsch, R. Schutte, S. Friedrich, I. Kistner, C. Ott, U. Raff, R. Veelken, and R. E. Schmieder, "Circadian rhythm and day to day variability of serum potassium concentration: A pilot study," *J. Nephrol.*, vol. 28, no. 2, pp. 165–172, Apr. 2015.
[35] F. Badilini, M. Vaglio, R. Dubois, P. Roussel, N. Sarapa, I. Denjoy, F. Extramiana, and P. Maison-Blanche, "Automatic analysis of cardiac repolarization morphology using Gaussian mesa function modeling," *J. Electrocardiol.*, vol. 41, no. 6, pp. 588–594, Nov. 2008.
[36] J. V. Candy, *Model-Based Signal Processing*, 1st ed. Hoboken, NJ, USA: Wiley, 2006.
[37] G. I. Sandle, E. Gaiger, S. Tapster, and T. H. J. Goodship, "Evidence for large intestinal control of potassium homoeostasis in uraemic patients undergoing long-term dialysis," *Clin. Sci.*, vol. 73, no. 3, pp. 247–252, Sep. 1987.
[38] G. Giebisch, R. Krapf, and C. Wagner, "Renal and extrarenal regulation of potassium," *Kidney Int.*, vol. 72, no. 4, pp. 397–410, Aug. 2007.
[39] G. H. Williams, J. P. Cain, R. G. Dluhy, and R. H. Underwood, "Studies of the control of plasma aldosterone concentration in normal man," *J. Clin. Invest.*, vol. 51, no. 7, pp. 1731–1742, Jul. 1972.
[40] S. Patnaik and Y. K. Lai, "Just hypercalcaemia or acute ST elevation myocardial infarction? A review of hypercalcaemia-related electrocardiographic changes," *BMJ Case Rep.*, vol. 2015, Oct. 2015, Art. no. bcr2015211177, doi: 10.1136/bcr-2015-211177.
[41] A. Martinez-Vea, A. Bardají, C. Garcia, and J. A. Oliver, "Severe hyperkalemia with minimal electrocardiographic manifestations," *J. Electrocardiol.*, vol. 32, no. 1, pp. 45–49, Jan. 1999.
[42] D. Dreyfuss, G. Jondeau, R. Couturier, J. Rahmani, P. Assayag, and F. Coste, "Tall T waves during metabolic acidosis without hyperkalemia," *Crit. Care Med.*, vol. 17, no. 5, pp. 404–408, May 1989.
[43] L. Huber and F. J. Gennari, "Severe metabolic alkalosis in a hemodialysis patient," *Amer. J. Kidney Diseases*, vol. 58, no. 1, pp. 144–149, Jul. 2011.
[44] F. L. Coe, "Metabolic alkalosis," *J. Amer. Med. Assoc.*, vol. 238, no. 21, p. 2288, 1977.
[45] R. F. Reilly and M. A. Perazella, *Nephrology in 30 Days* (In Thirty Days Series), 2nd ed. New York, NY, USA: McGraw-Hill, Sep. 2013.
[46] Q. Qian, "Acid-base alterations in ESRD and effects of hemodialysis," *Seminars Dialysis*, vol. 31, no. 3, pp. 226–235, May 2018.
[47] M. Hernández Mesa, N. Pilia, O. Dössel, and A. Loewe, "Influence of ECG lead reduction techniques for extracellular potassium and calcium concentration estimation," *Current Directions Biomed. Eng.*, vol. 5, no. 1, pp. 69–72, Sep. 2019.
[48] R. Lampert, "ECG signatures of psychological stress," *J. Electrocardiol.*, vol. 48, no. 6, pp. 1000–1005, Nov. 2015.
[49] F. Akhras and A. F. Rickards, "The relationship between QT interval and heart rate during physiological exercise and pacing.," *Jpn. Heart J.*, vol. 22, no. 3, pp. 345–351, 1981.

ANA SANTOS RODRIGUES received the B.Sc. degree in bioengineering from the Faculty of Engineering of the University of Porto (FEUP), in 2015, specializing in biomedical engineering, and the M.Sc. degree in biomedical engineering from the Kaunas University of Technology (KTU), Kaunas, Lithuania, in 2017, where she is currently pursuing the Ph.D. degree with the Biomedical Engineering Institute. Her research interests include development of algorithms for noninvasive monitoring of chronic diseases, particularly biomedical signal processing for cardiovascular health assessment. Her current research interest includes developing unobtrusive biomarkers of homeostasis in hemodialysis patients.

ANDRIUS PETRĖNAS received the B.Sc. degree in electronics engineering, the M.Sc. degree in biomedical engineering, and the Ph.D. degree in electronics engineering from the Kaunas University of Technology (KTU), Kaunas, Lithuania, in 2009, 2011, and 2015, respectively. He is currently with the Biomedical Engineering Institute, KTU. His research interests include signal processing algorithms for long-term monitoring of heart arrhythmias, with particular interest in the detection of paroxysmal atrial fibrillation.

BIRUTĖ PALIAKAITĖ received the B.Sc. degree in biomedical engineering from the Kaunas University of Technology (KTU), Kaunas, Lithuania, in 2016 and 2018, respectively, where she is currently pursuing the Ph.D. degree with the Biomedical Engineering Institute. Her research interests include biomedical signal processing for cardiovascular health assessment in free-living conditions.

NEDA KUŠLEIKAITĖ-PERE received the M.D. degree from Vilnius University, in 1998, and the Ph.D. degree from the Lithuanian University of Health Sciences (LSMU), in 2011. She is currently working as a Nephrologist with the Hospital of LSMU Kauno Clinics and a Lecturer with LSMU. Her research interests include electrolyte disturbances, malnutrition, quality of life in patients with chronic kidney disease, and living donor kidney transplantation.

GEDIMINAS JARUŠEVIČIUS received the degree in medicine from the Kaunas Academy of Medicine, in 1992, having later completed his residentship in internal medicine in 1994. In 1996, he completed his residentship in cardiology and interventional cardiology in 1997. He also received the Ph.D. degree in medicine from the Kaunas University of Medicine, in 2000. He is currently a Professor with the Department of Cardiology, Medical Academy, Lithuanian University of Health Sciences (LSMU), Kaunas, Lithuania, an Interventional Cardiologist with Kaunas University Clinics, and a Researcher with the Institute of Cardiology, LSMU.

INGA ARŪNĖ BUMBLYTĖ is currently a Professor of nephrology with the Lithuanian University of Health Sciences (LSMU). She is also the Head of the Nephrology Department, Hospital of LSMU Kauno Clinics. She has been an Active Member of the Lithuanian association of Nephrology, Dialysis, and Transplantation (LNDTA) and a Council Member of LNDTA since 2005. She was elected as the President of LNDTA in 2015 and 2019. She has also been a Liaison officer with the ISN Sister Renal Centers program since 1997: Kaunas – Gent from 1997 to 2009; Brest – Kaunas – Gent from 2010 to 2015; and Luck – Brest – Kaunas since 2016. ERA-EDTA Distinguished Fellow awarded her in 2017. She has supervised five Ph.D. Thesis. Her research interests include electrolyte disorders and malnutrition in chronic kidney disease (CKD) patients, prognostic factors of severe acute kidney injury, risk factors of CKD in primary care, vascular calcification, and biomarkers in kidney transplantation.

PABLO LAGUNA (Fellow, IEEE) received the master's and Ph.D. degrees in biomedical engineering from the University of Zaragoza, Spain, in 2010 and 2020, respectively.

At the University of Zaragoza, he was the Vice-Dean for international relations from 1999 to 2002, and a Researcher with the Aragón Institute for Engineering Research (I3A), where he was responsible for the Biomedical Engineering Division from 2000 to 2011. He has been serving as the Director since 2019. He has served as a Scientific Director of the Spanish Center for Biomedical Engineering, Biomaterial, and Nano-medicine Research (CIBER-BBN), from 2011 to 2015. He is currently a Full Professor of signal processing and communications with the Department of Electrical Engineering, Engineering School, University of Zaragoza. His research interests include signal processing, in particular for biomedical applications. He has coauthored more than 150 research articles on this topic, over 300 international conference papers, and has advised 15 Ph.D. Thesis. He has lead several projects on biomedical signal interpretation, particularly in the cardiovascular domain, most of them with international collaborations at clinical and engineering sites. He is having some international scientific responsibilities as the Editor of the *Digital Signal Processing* journal (Eurasip), and the *Medical and Biological Engineering and Computing* (Springer). He had served as a member and the President of the board of directors of the Computing in Cardiology Society, organized different scientific conferences, and so on. He is also a Fellow of EAMBES and IAMBE. He is, together with L. Sörnmo, the author of the book entitled *Bioelectrical Signal Processing in Cardiac and Neurological Applications* (Elsevier, 2005).

VAIDOTAS MAROZAS (Member, IEEE) received the B.S., M.Sc., and Ph.D. degrees in electronics engineering from the Kaunas University of Technology, Kaunas, Lithuania, in 1993, 1995, and 2000, respectively. He has been a Coordinator of the biomedical engineering master's program since 2007, a Professor of the Department of Electronics Engineering since 2015, and the Director of the Biomedical Engineering Institute since 2016. His expertise is in developing devices and signal processing algorithms for personal health monitoring. He has led projects and contracts dedicated to the development of a wrist-worn device for heart arrhythmia monitoring, tools for studying hypotension and diver's physiology, and monitoring mental stress. He was a Visiting Scientist in Lund (Sweden) and Zaragoza (Spain) universities. He has coauthored more than 30 scientific journal articles and over 60 conference papers. He is also supervising three Ph.D. students.